

# A Multi-AUV State Estimator for Determining the 3D Position of Tagged Fish

Yukun Lin<sup>1</sup>, Hannah Kastein<sup>2</sup>, Taylor Peterson<sup>3</sup>, Connor White<sup>4</sup>,  
Christopher G. Lowe<sup>5</sup> and Christopher M. Clark<sup>6</sup>

**Abstract**—This paper presents a multi-AUV state-estimator that can determine the 3D position of a tagged fish. In addition to angle measurements, the state-estimator also incorporates distance and depth measurements. These additional sensor measurements allow for greater accuracy in the position estimates. A newly developed motion model that better accounts for multiple hypotheses of the motion of a tagged fish is used to increase the robustness of the state-estimator. A series of multi-AUV shark tracks were conducted at Santa Catalina Island, California over the span of four days to demonstrate the ability of the state-estimator to determine the 3D position of a tagged leopard shark. Additional experiments in which the AUVs tracked a tagged boat of known location were conducted to quantify the performance of the presented state-estimator. Experimental results demonstrate a three-fold decrease in mean state-estimation error compared to previous works.

## I. INTRODUCTION

Studying the spatial movement of sharks and other fishes is an important tool for monitoring habitat and maintaining fish populations. Typical methods for tracking fish include tagging individuals with acoustic transmitters, and then using hydrophone-receiver systems to detect and measure the signals transmitted. Often, the hydrophone-receivers are placed at fixed locations around an environment of interest to passively track tagged individuals that move through the static array [1]. Alternatively, active tracking can be done manually by mounting a directional hydrophone on a boat and continuously following the tagged individual from the surface for periods up to 96 h [2].

To enable active tracking without the need for human operators, the authors have demonstrated in previous works that a multi-AUV system using only low resolution angle measurements is able to autonomously track and follow tagged leopard sharks [3]. A key component of this system is a state-estimator which determines the 2D position of the tagged shark [4]. In order to provide more sensor

measurements that can be incorporated by the state-estimator, the authors have also developed a method of calculating the distance-to-tag [5]. The work presented here expands on these previous works. Its contributions include:

- 3D position estimates of the tagged fish.
- The incorporation of distance and depth measurements into the state-estimator.
- Increased accuracy in position estimates.
- A new motion model that is able to better account for multiple hypothesis of the motion of a tagged fish.
- Demonstration of the state-estimator in real shark tracking over an extended period of time in Big Fishermans Cove, Catalina Island, California, and additional boat track experiments to validate the performance of the state-estimator.

The paper is organized as follows. Section II describes the past work and related research on the topic. Sections III gives an overview of the multi-AUV system, and Section IV presents the state-estimator. Sections V and VI describe the experiments performed at Catalina Island that demonstrate effectiveness of the state-estimator.

## II. BACKGROUND

Tracking stationary and moving targets with robotic systems is a well-studied field of research [6], [7], [8], [9], [10], [11]. Within the context of using underwater robots to track individuals, both optical based methods [12], [13], [14], and acoustic based methods [15], [16] have been used. In [12] autonomous tracking of jellyfish with an ROV was conducted using basic image processing techniques. Work presented in [13] demonstrated the use of SIFT features in tracking individual fish between video frames captured from an ROV. Image processing techniques were also shown to be useful in tracking divers with a robot in [14]. Unfortunately, most optical methods employed in underwater environments suffer from limited visibility due to poor lighting conditions and presence of debris.

While acoustic methods of tracking marine individuals have been used for decades, hydrophone receivers have only recently been mounted on underwater vehicles. For example, work done by [11], [15] has demonstrated the ability to track tagged sturgeon using a REMUS AUV equipped with a Lotek hydrophone system. Unlike the work presented by the authors, work by [11], [15] did not use in-situ measurements to actively steer the AUV.

One problem encountered during state-estimation is the inability to geometrically determine the position of the

<sup>1</sup>Yukun Lin is with Department of Computer Science and Mathematics, Harvey Mudd College, Claremont, CA 91711 ylin@hmc.edu

<sup>2</sup>Hannah Kastein is with the Department of Engineering, Harvey Mudd College, Claremont, CA 91711 hkastein@hmc.edu

<sup>3</sup>Taylor Peterson is with the Department of Engineering and Computer Science, Harvey Mudd College, Claremont, CA 91711 tpeterson@hmc.edu

<sup>4</sup>Connor White is with the Department of Biological Sciences, California State University Long Beach, Long Beach, CA 90840 connor.white@student.csulb.edu

<sup>5</sup>Christopher G. Lowe is with the Department of Biological Sciences, California State University Long Beach, Long Beach, CA 90840 clowe@csulb.edu

<sup>6</sup>Christopher M. Clark is with the Department of Engineering, Harvey Mudd College, Claremont, CA 91711 clark@hmc.edu

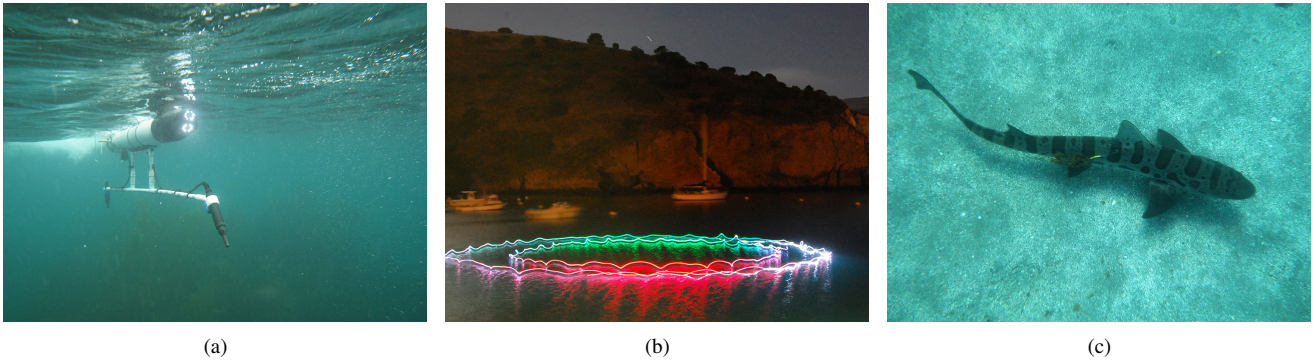


Fig. 1. Hydrophones mounted on a prototype PVC frame attached to an OceanServer Iver2, suspended 0.4 m down with 2.4 m of separation is shown in (a). The two AUVs circling in (b) are tracking the tagged leopard shark shown in (c)

tag using the sensor measurements. To address this issue, Monte Carlo Localization (MCL) methods have been used in the past [17], [18], [19], [20], [21], [22]. Unfortunately, traditional MCL methods suffer from the particle deprivation problem; variants of MCL that handle particle deprivation include [23], [24]. A genetic filter presented by [23] uses residual mutation to “push” lost particles towards the true state. Adaptive Monte Carlo Localization (aMCL) presented by [24] adds random particles based on the long- and short-term likelihoods of sensor measurements to prevent clustering of particles in wrong locations. The adaptive hybrid motion model presented in this paper builds on these works.

The authors are also aware of the tracking of a White Shark using a REMUS-100 AUV conducted by researchers at the Woods Hole Oceanographic Institute (WHOI). Their work was featured by Discovery Channel in 2013. In their approach, a cylindrical transponder approximately 30 cm long is used as a tag. An Ultra-Short BaseLine receiver mounted on the REMUS-100 AUV queries the transponder to determine range and bearing. Our approach uses much smaller off-the-shelf Lotek acoustic tags that are only capable of pulse transmission. While bearing and range measurements obtained from these tags tend to be less accurate than that of a transponder, the small size of these tags makes them applicable to a large variety of smaller fish. Our system also attempts to minimize any changes in behavior of the shark being tracking by using a controller that circles and maintains a predetermined buffer distance from the shark instead of getting as close as possible.

This paper presents a state-estimator capable of determining the 3D position of a tagged fish by incorporating new sensor measurements. A new motion model, combined with the incorporation of additional sensor measurements, allows the state-estimator to localize the tag with increased accuracy.

### III. SYSTEM OVERVIEW

The state estimator is part of a multi-AUV system capable of following and tracking a tagged fish. The system consists of two OceanServer Iver2 AUVs, a torpedo-shaped vehicle (see Fig. 1(a)) with a rear propeller to provide locomotion, and four fins to control the vehicle’s pitch, row and yaw. It is equipped with two processors, a primary and secondary,

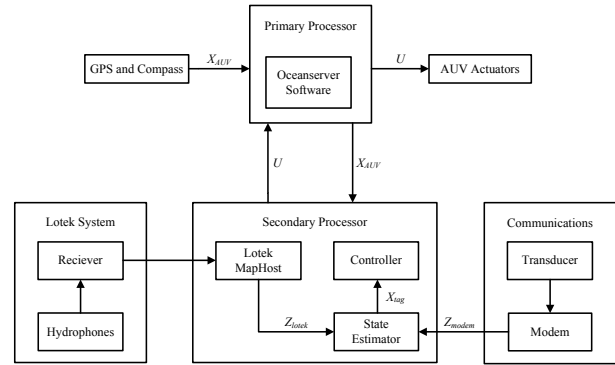


Fig. 2. Flow control within an AUV.

each running an embedded Windows operating system. The primary processor communicates with the AUV’s sensors and actuators. The secondary processor interfaces with the primary via serial and hosts the user programmed control, estimation and communication systems. The AUVs share its current position and sensor measurements with each other via a WHOI Micro-Modem [25] and externally mounted transducers, allowing for cooperative tracking and following of the tagged marine animal.

The flow control within each AUV is shown in Fig. 2. The estimated state of the tagged fish is passed to a decentralized target circumnavigational controller described in detail in [26]. The AUVs will circumnavigate the current estimate of the tag position (see Fig. 1(b)), and transition to circumnavigate a newer estimate of the tag position when it has moved past a threshold distance from the last position being circumnavigated. The AUVs transition from the older circumnavigation position to the newer one by travelling in a straight line. If a tag position estimate is outside of the defined safe boundary, the AUVs will circumnavigate the closest point on the boundary instead. Currently, the control system only does circumnavigation on the surface, but will be extended in the future to circumnavigate underwater.

The sensor payload used to determine the AUV state includes a 3-DOF compass, a wireless antenna, a GPS receiver,

and a 6-beam Doppler Velocity Logger. Each AUV is also outfitted with a Lotek MAP600RT receiver and an associated stereo-hydrophone set, designed to listen for acoustic signals at a frequency of 76 kHz. These allow the vehicles to receive transmissions from Lotek MM-M-16-50-PM acoustic tags, which transmit at 76.8 kHz. The tag has a pressure sensor and its readings are encoded into the tag transmission. Depth is calculated from pressure reading using linear extrapolation. The two hydrophones of the stereo-hydrophone system are mounted 2.4 m apart and suspended 0.4 m beneath each AUV. The separation of the hydrophones allows the angle between the AUV and the acoustic tag to be calculated by the Lotek MapHost software.

Due to the periodic nature of the tag transmissions, it is possible to extrapolate and predict the time of transmission from some initial transmission time and the transmission period [5]; this allows the distance-to-tag to be calculated using time-of-flight. The specifics are presented in [5] and experimental results in [5] show that the calculated distance has an error with a mean and standard deviation on the order of 2 m over a time span of 4 h, with a drift of 1.5 m over a time span of 22 h.

#### IV. STATE ESTIMATOR

##### A. State Estimation Problem

An overview of the state estimation problem is shown in Fig. 3. The state of the  $i^{th}$  AUV and sensor measurements at time  $t$  are denoted by  $X_{auv,t}^i$  and  $Z_t^i$ , respectively. The hydrophones  $h_1$  and  $h_2$  are mounted on the nose and tail ends of the AUV and the difference in time of arrival of a tag transmission is used by the Lotek MapHost software to calculate the angle to the tag (with a sign ambiguity), denoted by  $z_\alpha^i$ . Using the time of arrival measurement, the distance-to-tag  $z_\beta^i$  can be calculated. The depth of the tag  $z_\gamma^i$  is determined using the measurement transmitted from the tag.

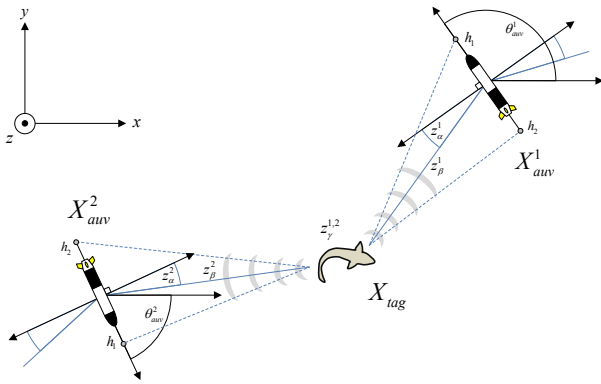


Fig. 3. An overview of the state estimation problem.

The multi-AUV state estimation problem is defined as follows. Given a system of  $n$  AUVs at time  $t$  where the

$i^{th}$  AUV has the state

$$X_{auv,t}^i = [x_{auv}^i \ y_{auv}^i \ z_{auv}^i \ \theta_{auv}^i]_t \quad (1)$$

and sensor measurements

$$Z_t^i = [z_\alpha^i \ z_\beta^i \ z_\gamma^i]_t, \quad (2)$$

determine the tag state

$$X_{tag,t} = [x_{tag} \ y_{tag} \ z_{tag}]_t. \quad (3)$$

The state estimator must also handle incomplete sensor measurements, such as the case of  $Z_t^i$  only containing a valid distance measurement  $z_\beta^i$  but invalid angle and depth measurements.

##### B. Particle Filter Overview

The state-estimator is based on a particle filter [22], [24]. To represent the belief state at time  $t$ , the particle filter uses a set of particles denoted by  $P_t$ . Each particle  $p \in P_t$  represents the set  $\{X_{tag}^p, w^p\}$  containing a tag state  $X_{tag}^p$  and weight  $w^p$ . The tag state  $X_{tag,t}$  is the average of  $X_{tag}^p \in p$  of all  $p \in P_t$ . At initialization,  $P_t$  is filled with particles whose  $xyz$  coordinates are sampled randomly from uniform distributions. The algorithm for the state-estimator is shown in Alg. 1.

---

##### Algorithm 1 Multi-AUV State Estimator

---

```

1: //Prediction
2: for  $p \in P_t$  do
3:    $X_{tag}^p \in p \leftarrow \text{Motion\_Model}(X_{tag}^p)$ 
4:   for  $i$  from 1 :  $n$  do
5:      $\alpha_{exp}^p \leftarrow \text{Vector\_Angle}(X_{auv,t}^i, X_{tag}^p)$ 
6:      $\beta_{exp}^p \leftarrow \text{Euclidean\_Dist}(X_{auv,t}^i, X_{tag}^p)$ 
7:      $\gamma_{exp}^p \leftarrow z_{tag} \in X_{tag}^p$ 
8:      $w_p \leftarrow W(z_\gamma^i, \gamma_{exp}^p, \sigma_\gamma) * W(z_\beta^i, \beta_{exp}^p, \sigma_\beta) * W(z_\alpha^i, \alpha_{exp}^p, \sigma_\alpha)$ 
9:   end for
10: end for

11: //Correction
12: if there are valid measurements then
13:   for 1 :  $|P_t|$  do
14:     choose  $p \in P_t$  with probability  $\propto w_p$ 
15:     add  $p$  to  $P_{t+1}$ 
16:   end for
17: else
18:    $P_{t+1} \leftarrow P_t$ 
19: end if

```

---

At each time step, the set of particles is propagated based on a motion model (Alg. 1, line 3). The particle weights  $w_p$  are calculated using the  $n$  AUV states and corresponding sensor measurements (Alg. 1, line 5-8). The expected angle measurement  $\alpha_{exp}^p$  (Alg. 1, line 5) is calculated by subtracting  $\pi/2$  from the angle between the two vectors

$$\vec{\theta} = [\cos(\theta_{auv}^i), \sin(\theta_{auv}^i), 0]$$

TABLE I  
MOTION MODEL AND WEIGHT FUNCTION PARAMETERS.

Parameter	$\sigma_v$ (m/s)	$\sigma_{vz}$ (m/s)	$k$ (m/s)	$\lambda$ (m/s)	$\rho$	$\alpha_{slow}$	$\alpha_{fast}$	$\phi$	$\sigma_\alpha$ (rad)	$\sigma_\gamma$ (m)	$\sigma_\beta$ (m)
Value	1	0.8	0.5	1	0.66	0.05	0.5	0.025	$\pi/18$	0.75	2

---

**Algorithm 2** Hybrid Random Walk Motion Model

---

```

1:  $\theta_{tag}^p \leftarrow \text{UniformDistribution}(0, 2\pi)$ 
2:  $v_{tag}^z \leftarrow \text{NormalDistribution}(0, \sigma_{vz})$ 
3: //  $\rho$  is a number between 0 and 1
4: if  $\rho \geq \text{UniformDistribution}(0, 1)$  then
5:    $v_{tag}^{xy} \leftarrow \text{ParetoDistribution}(k, \lambda)$ 
6: else
7:    $v_{tag}^{xy} \leftarrow \text{Abs}(\text{NormalDistribution}(0, \sigma_v))$ 
8: end if
9:  $x_{tag}^p \leftarrow x_{tag}^p + |v_{tag}^{xy}| \cos(\theta_{tag}^p) \Delta t$ 
10:  $y_{tag}^p \leftarrow y_{tag}^p + |v_{tag}^{xy}| \sin(\theta_{tag}^p) \Delta t$ 
11:  $z_{tag}^p \leftarrow z_{tag}^p + v_{tag}^z \Delta t$ 

```

---

and

$$\vec{p} = [x_{auv}^i - x_{tag}^p, y_{auv}^i - y_{tag}^p, z_{auv}^i - z_{tag}^p].$$

The weighting function  $W$  implements a Gaussian probability density function [17]. If there are valid measurements, the particles are re-sampled based on their weights to create a new set of particles (Alg. 1, line 13-16). The following subsections go into more detail about the main functions used in Alg. 1.

### C. Hybrid Motion Model

Due to lack of odometry from the tag, a stochastic motion model is used in the prediction step of the state-estimator to propagate the particles. The motion model used is described in Alg. 2 and builds upon [3]. It is best described as a hybrid Brownian and Levy Flight motion model.

The Brownian random walk motion model draws its step length from a normal distribution centered at 0 and the direction of the step from a uniform distribution with interval  $[0, 2\pi]$ . Due to the exponential tail of the normal distribution, the likelihood of a long step is extremely low. The problem arises during extended periods of time without valid sensor measurements. During these periods, there tends to be a higher probability of the tagged fish moving to a new location. If this happens, the inability of the Brownian motion model to simulate long jumps often means that none of the particles will be near the vicinity of the true location of the tagged fish when a new sensor measurement is obtained. Thus, extended periods without valid sensor measurements lead to particle deprivation and degrade the performance of the state-estimator.

In contrast, the Levy Flight random walk motion model draws its step length from a tail heavy distribution. However, it often over-compensates for the weakness of the Brownian motion model by spreading out the particles too aggressively.

---

**Algorithm 3** Determining  $\rho$  adaptively

---

```

1: static  $w_{slow}, w_{fast}, \tau$ 
2: if there are valid measurements then
3:    $w_{avg} \leftarrow \frac{1}{|P_t|} \sum(w^p \in P_t)$ 
4:    $w_{slow} \leftarrow w_{slow} + \alpha_{slow}(w_{avg} - w_{slow})$ 
5:    $w_{fast} \leftarrow w_{fast} + \alpha_{fast}(w_{avg} - w_{fast})$ 
6:    $\rho \leftarrow \max(0, 1 - w_{fast}/w_{slow}, \text{Clip}(\tau * \phi, 0, 1))$ 
7: end if

```

---

This degrades the performance of the state-estimator when the tagged fish is loitering around slowly or almost stationary.

The hybrid Brownian and Levy flight motion model addresses the weaknesses of using solely the Brownian or Levy flight motion models. In lines 4-8 of Alg. 2, the motion model chooses with probability  $\rho$  and  $1 - \rho$  of using a tail heavy (Pareto distribution with scale and shape parameter of  $k$  and  $\lambda$  respectively) or normal distribution in determining step length respectively. By using an appropriate value of  $\rho$ , the weakness of the Brownian flight motion model is compensated by the Levy flight motion model and vice-versa. There are two possible ways of determining  $\rho$ .

1) *Hybrid Fixed*: The probability  $\rho$  can be fixed using a priori knowledge about the motions of the tagged fish.

2) *Hybrid Adaptive*: An alternative to fixing the probability  $\rho$  is to adjust it adaptively. Drawing from aMCL in [24],  $\rho$  can be adjusted by comparing the short and long term average of the likelihood of sensor measurement  $Z_t^i$ . This requires adding an addition step right after the correction step in Alg. 1 and is shown in Alg. 3. The number of time steps since a valid measurement was received, denoted by  $\tau$ , is also taken into account in line 6 of Alg. 3; the Clip function limits  $\tau * \phi$  to the interval  $[0, 1]$ . Thus, if no measurements were received after  $1/\phi$  time steps or more, the motion model will always draw its step length from the tail heavy distribution.

### D. Weight Function

For some measurement  $z_s$ , where  $s \in \{\alpha, \beta, \gamma\}$ , with expected measurement  $s_{exp}^p$  and standard deviation  $\sigma_s$  corresponding to particle  $p$ , the weight function (Alg. 1, line 8) implements a Gaussian distribution function given by

$$W(z_s, s_{exp}^p, \sigma_s) = \frac{1}{\sqrt{2\pi}\sigma_s} e^{-\frac{(s_{exp}^p - z_s)^2}{2\sigma_s^2}}. \quad (4)$$

For  $z_\alpha, z_\beta$  and  $z_\gamma$ , the standard deviations used are determined experimentally and shown in Table I.

## V. EXPERIMENTS

A series of verification experiments were performed at Big Fisherman's Cove, Catalina Island, CA. The cove is adjacent to the USC Wrigley Institute of Environmental Studies.

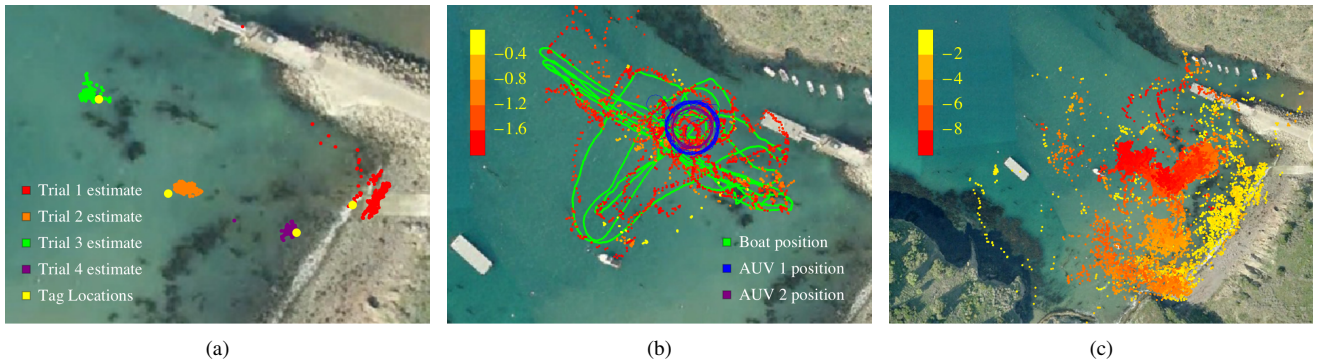


Fig. 4. Result of stationary, boat and shark trials shown in (a), (b) and (c) respectively. In (b) and (c), the estimated tag locations are shown by the dots ranging from yellow to red, which corresponds to estimated tag depth (m) shown in the bar legend. Even though the tag was held by a fixed length line in (b), movement of the boat caused the tag to rise up.

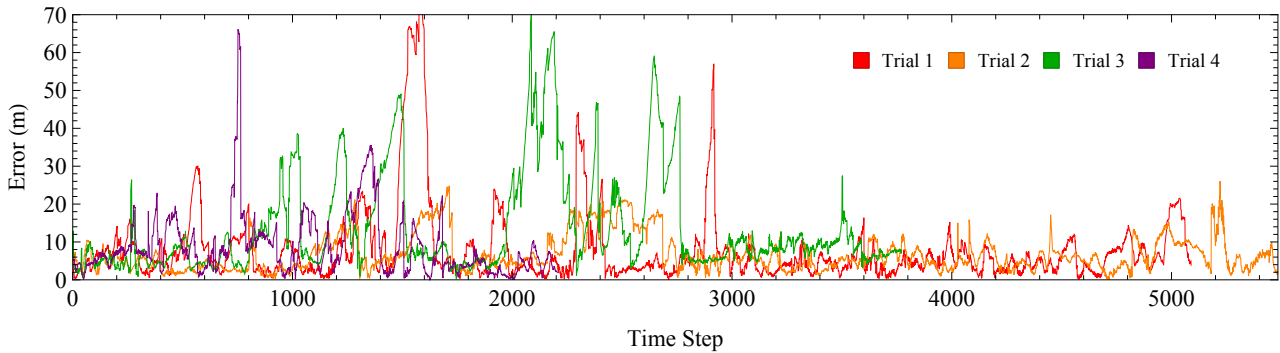


Fig. 5. Boat track errors as a function of time.

The first set of experiments referred to as the *Static Trials* was conducted on 5 October 2013. A tag was placed on the sea floor at depths ranging from 2m to 8m, and its location was recorded with a GPS receiver. A single AUV was deployed to simultaneously estimate tag position and circle this estimated position.

The second set of experiments referred to as the *Boat Trials* was conducted on 18 January 2014. A tag was hung from a moving boat with a 2m line. Both AUVs were set to circle a fixed point, and the boat was driven around the cove at various speeds up to  $2.0\text{ms}^{-1}$ . The recorded measurements from the AUVs were then post-processed offline by the presented state-estimator. The true state of the boat was recorded by a GPS receiver.

The third set of experiments is referred to as the *Shark Trials*. A leopard shark was tagged and tracked from 15-18 July 2013 at different time intervals and 12.5 h of 3D location data was obtained.

## VI. RESULTS AND DISCUSSION

In the *Static Trials* and *Shark Trials*, an older state-estimator was used for online tracking, and the measurements obtained were then post processed with the new state-estimator described above. In the *Boat Trials*, the measurements were post processed to correct for delays due to the low latency (10s per 32 bytes) of the acoustic modems.

TABLE II  
STATE ESTIMATION ERRORS OF STATIC AND BOAT TRIALS.

Trial	Mean Err. (m)		Median Err. (m)		SD Err. (m)	
	Static	Boat	Static	Boat	Static	Boat
1	8.1	8.0	7.2	5.0	4.3	10.5
2	4.8	6.8	4.6	5.3	1.6	4.8
3	3.7	13.7	3.6	8.4	1.1	13.2
4	2.8	8.8	2.0	6.5	3.4	8.4

### A. Static Trials

A total of four stationary trials were conducted and the results are shown in Fig. 4(a). In trial 1, the tag was placed at a location outside the region that the AUV was allowed to circle. Thus, the AUV circled a point on the boundary that was nearest to the estimated tag location. As successful angle measurements require both hydrophones to get good detections, increased distances or blocked line of sight increases the likelihood of failed angle measurements; in the case of trial 1, these factors lead to a 99% failure rate for angle measurements during trial 1, causing the higher mean error of 8.1m shown in Table II.

### B. Boat Trials

A total of four boat trials were conducted and the only results of trial 1 is shown in Fig. 4(b). The state estimation errors of all four trials are shown in Table II and Fig. 5. For trial 1, a mean error of 8.0m was obtained. An approximation

TABLE III  
COMPARISON OF ERRORS USING DIFFERENT MOTION MODELS.

Motion Model	Mean Err. (m)		Median Err. (m)		2nd Quartile (m)		3rd Quartile (m)		Max Err. (m)		SD Err. (m)	
	Static	Boat	Static	Boat	Static	Boat	Static	Boat	Static	Boat	Static	Boat
Hybrid Fixed	7.6	8.9	5.9	5.9	3.7	3.5	8.9	10.2	105.1	115.7	8.0	9.7
Hybrid Adaptive	8.8	9.6	6.0	6.2	4.1	3.7	9.3	10.7	109.1	113.5	10.5	10.9
Brownian	7.5	27.2	5.2	14.2	3.4	5.7	7.9	42.9	103.6	154.2	9.4	28.8
Levy	10.0	8.8	8.1	5.8	4.4	3.5	12.3	10.1	108.0	117.0	9.8	9.5

TABLE IV  
PERFORMANCE WITH AND WITHOUT DISTANCE MEASUREMENTS.

Trial	Mean Err. (m)		Median Err. (m)		SD Err. (m)	
	Dist.	No Dist.	Dist.	No Dist.	Dist.	No Dist.
1	7.6	27.4	4.8	20.2	9.3	23.7
2	6.9	19.8	5.3	16.0	5.0	17.3
3	13.5	34.5	7.9	29.6	13.8	23.5
4	9.2	29.7	6.8	26.4	8.5	20.9

TABLE V  
COMPARISON OF RECOVERY TIMES.

Motion Model	Mean Recovery Time (time steps)				
	15 m	30 m	45 m	60 m	75 m
Hybrid Fixed	38	49	82	58	132
Hybrid Adaptive	34	60	90	68	65
Brownian	70	171	291	1142	1511
Levy	39	44	53	61	70

of the state-estimation error  $\epsilon_t$  at time  $t$  is calculated by

$$\epsilon_t = \sqrt{\text{IQR}_x^2 + \text{IQR}_y^2}, \quad (5)$$

where  $\text{IQR}_x$  and  $\text{IQR}_y$  are the interquartile range of the  $x$  and  $y$  coordinates of the particles at time  $t$ . Let  $e_t$  be the actual error at time  $t$ . The distribution of  $\epsilon_t - e_t$  for the boat trials resembles a Gaussian with mean and standard deviation of 1.4 m and 10.9 m respectively. This suggests that while  $\epsilon_t$  may not be a reliable approximation of error at each time step, it can provide a good approximation of the overall error of a track. Indeed, the overall mean error of the boat trials in Table II is 9.0 m, and the approximation of the overall mean error is 10.4 m. Being able to approximate the state-estimation error is important when there are no truth measurements, such as during the tracking of a tagged shark.

### C. Shark Trials

The result of the shark trials are shown in Fig. 4(c), which aggregates the data from 6 individual tracks. Within these tracks, the amount of time in which the AUVs were circling the estimated shark position versus the amount of time in which the AUVs were circling a point on the boundary is roughly equal. Using Eq. 5, the overall mean and median error of the shark trials are approximated to be 12.9 m and 7.5 m respectively. The standard deviation of these errors is approximated to be 14.9 m. It is observed that shark locations were not distributed uniformly across the cove, instead locations were aggregated. With the addition of the 3D location data it is observed that the shark's depth is associated with the sea floor, as evidenced by deeper depths in deeper areas of the cove. Both of these observations agree with the known behavior of leopard sharks [27].

### D. Effect of Distance Measurements on Performance

To test the effect of incorporating distance measurements on the performance of the state-estimator, measurements from the boat trial were post processed with and without distance measurements. This was repeated 40 times for each

trial, and the results are shown in Table IV. By incorporating distance measurements, mean state-estimation errors were driven down by a factor of 3.6, 2.9, 2.6 and 3.2 for boat trials 1, 2, 3 and 4 respectively. This demonstrates a level of accuracy that was previously unobtainable.

### E. Comparison of Motion Models

1) *State-Estimation Error*: Measurements from all four boat trials were post processed 50 times for each motion model to compare the effect of each motion model on state-estimation errors. The results are summarized in Table III. For the boat trial, the Brownian motion model suffered from poor performance due to its inability to spread out particles fast enough during time intervals without sensor measurements, causing it to have the higher mean error of 27.2 m. Even though the Levy flight motion model has similar performance to the hybrid motion models in the boat trials, its aggressiveness in spreading out particles led to the higher mean error of 10.0 m for the static trials. In contrast, the Hybrid Fixed motion model performed better, with mean errors of 7.6 m and 8.9 m for the stationary and boat trials respectively. The difference between the mean error of the Hybrid Adaptive and Hybrid Fixed motion models is statistically significant according to a t-test; even though the Hybrid Adaptive motion model performed slightly worse, it has the advantage of requiring less a priori knowledge about the tagged target.

2) *Recovery*: State and sensor measurements from trial 2 of the stationary trials were used to investigate the speed of recovery of the state-estimator from bad estimates. Particle deprivation was artificially introduced by placing a cluster of particles of radius 1 m at different distances from the true tag location at some random time step during the trial, simulating the case of a tagged fish moving rapidly from its previous location to a new location. This was repeated 50 times for each motion model tested. A recovery by the state-estimator is defined as when the estimated tag location is within a 5.5 m radius of the true tag location. The results are shown

in Table V. As expected, the Brownian motion model took the longest time to recover, taking an average of 1142 time steps when the initial particle cluster is 60 m from the true tag location. In contrast, the Hybrid Fixed, Hybrid Adaptive and Levy flight motion models had shorter mean recovery times of 58, 68 and 61 time steps respectively when the initial particle cluster is 60 m from the true tag location.

## VII. CONCLUSIONS AND FUTURE WORK

The presented system represent a new state-estimator capable of determining the 3D position of a fish tagged with small, off-the-shelf acoustic transmitters. In trials during which the true position of the tag was known, comparisons show that using the newly developed hybrid motion model can improve performance and robustness of the state estimator. It is also shown that incorporating distance measurements can drive down state-estimation errors by a factor of three.

Future work will attempt to further drive down the state-estimation errors by using tags with inertial measurement units. The acceleration data from the tags can then be incorporated into the motion model, potentially leading to more accurate location estimates for time intervals that lack other sensor measurements.

## ACKNOWLEDGMENT

This material is based upon work supported by the National Science Foundation under Grant No. 1245813. This work was performed in part at the Claremont Colleges' Robert J. Bernard Biological Field Station. This work was performed in part using hex, a parallel-computing system operated by Harvey Mudd College's Department of Mathematics and made available through a grant from the W.M. Keck Foundation.

## REFERENCES

- [1] M. Espinoza, T. J. Farrugia, D. M. Webber, F. Smith, and C. G. Lowe, "Testing a new acoustic telemetry technique to quantify long-term fine-scale movements of aquatic animals," *Fisheries Research*, vol. 108, pp. 364–371, 2011.
- [2] C. G. Lowe and R. N. Bray, "Fish movement and activity patterns," in *The Ecology of California Marine Fishes*. Berkeley, California: University of California Press, 2006, pp. 524–553.
- [3] C. M. Clark, C. Forney, E. Manii, D. Shinzaki, C. Gage, M. Farris, C. G. Lowe, and M. Moline, "Tracking and following a tagged leopard shark with an autonomous underwater vehicle," *Journal of Field Robotics*, vol. 30, 2013.
- [4] D. Shinzaki, C. Gage, S. Tang, M. Moline, B. Wolfe, C. G. Lowe, and C. M. Clark, "A multi-aUV system for cooperative tracking and following of leopard sharks," in *Proceedings of the IEEE International Conference on Robotics and Automation*, 2013.
- [5] Y. Lin, H. Kastein, T. Peterson, C. White, C. G. Lowe, and C. M. Clark, "Using time of flight distance calculations for tagged shark localization with an aUV," in *Proceedings of the Unmanned Untethered Submersible Technology Conference*, 2013.
- [6] D. Schulz, W. Burgard, D. Fox, and A. Cramers, "Tracking multiple moving objects with a mobile robot," in *Computer Vision and Pattern Recognition, IEEE Computer Society Conference*, 2001.
- [7] D. Schulz, W. Burgard, D. Fox, and A. Cremers, "People tracking with mobile robots using sample-based joint probabilistic data association filters," *The international Journal of Robotics Research*, vol. 22, 2003.
- [8] M. Kobilarov, G. Sukhatme, J. Hyams, and P. Batavia, "People tracking and following with mobile robot using an omnidirectional camera and a laser," in *Proceedings of the 2006 IEEE International Conference on Robotics and Automation*, 2006.
- [9] M. Montemerlo, S. Thrun, and W. Whittaker, "Conditional particle filters for simultaneous mobile robot localization and people-tracking," in *Proceedings of the 2002 IEEE International Conference on Robotics and Automation*, vol. 1, 2002, pp. 695–701.
- [10] J. Rife and S. M. Rock, "Segmentation methods for visual tracking of deep-ocean jellyfish using a conventional camera," *IEEE Journal of Ocean Engineering*, vol. 28, pp. 595–608, 2003.
- [11] T. Grothues, J. Dobarro, and J. Eiler, "Collecting, interpreting, and merging fish telemetry data from an aUV: Remote sensing from an already remote platform," in *Autonomous Underwater Vehicles (AUV), 2010 IEEE/OES*, Monterey, CA, 2010, pp. 1–9.
- [12] J. Rife and S. M. Rock, "Segmentation Methods for Visual Tracking of Deep-Ocean Jellyfish using a Conventional Camera," *IEEE Journal of Oceanic Engineering*, vol. 28, no. 4, pp. 595–608, 2003.
- [13] J. Zhou and C. M. Clark, "Autonomous fish tracking by ROV using monocular camera," *Computer and Robot Vision, Canadian Conference*, vol. 0, p. 68, 2006.
- [14] C. Georgiades, A. German, A. Hogue, H. Liu, C. Prahacs, A. Ripsman, R. Sim, L. Torres, P. Zhang, M. Buehler *et al.*, "Aqua: an aquatic walking robot," in *Intelligent Robots and Systems, 2004.(IROS 2004). Proceedings. 2004 IEEE/RSJ International Conference on*, vol. 4. IEEE, 2004, pp. 3525–3531.
- [15] T. M. Grothues, J. Dobarro, J. Ladd, A. Higgs, G. Niezgod, and D. Miller, "Use of a multi-sensored aUV to telemeter tagged Atlantic sturgeon and map their spawning habitat in the Hudson river, USA," in *Autonomous Underwater Vehicles, 2008. AUV 2008. IEEE/OES*, Woods Hole, MA, 2008, pp. 1–7.
- [16] M. J. Oliver, M. W. Breece, D. A. Fox, D. E. Haulsee, J. T. Kohut, J. Manderson, and T. Savoy, "Shrinking the haystack: using and aUV in an integrated ocean observatory to map Atlantic sturgeon in the coastal ocean," *Fisheries*, vol. 38, 2013.
- [17] C. Forney, E. Manii, M. Farris, M. Moline, C. G. Lowe, and C. M. Clark, "Tracking of a tagged leopard shark with an aUV: Sensor calibration and state estimation," in *Proceedings of the 4th International Conference on Robotics and Automation*, 2012.
- [18] S. Thrun, D. Fox, W. Burgard, and F. Dellaert, "Robust Monte Carlo localization for mobile robots," *Artificial Intelligence*, vol. 128, no. 1-2, pp. 99–141, 2001.
- [19] D. Fox, S. Thrun, W. Burgard, and F. Dellaert, "Particle filters for mobile robot localization," 2001.
- [20] F. Gustafsson, F. Gunnarsson, N. Bergman, U. Forssell, J. Jansson, R. Karlsson, and P. Nordlund, "Particle filters for positioning, navigation, and tracking," *IEEE Transactions on Signal Processing*, vol. 50, no. 2, pp. 425–437, 2002.
- [21] D. Fox, W. Burgard, F. Dellaert, and S. Thrun, "Monte Carlo localization: Efficient position estimation for mobile robots," in *Proceedings of the National Conference on Artificial Intelligence*, 1999, pp. 343–349.
- [22] S. Thrun, "Particle filters in robotics," in *Proceedings of the 17th Annual Conference on Uncertainty in AI (UAI)*, vol. 1, 2002.
- [23] S. Park, J. Hwang, K. Rou, and E. Kim, "A new particle filter inspired by biological evolution: Genetic filter," *World Academy of Science, Engineering and Technology*, vol. 33, 2007.
- [24] S. Thrun, W. Burgard, and D. Fox, *Probabilistic Robotics*. Cambridge, MA: The MIT Press, 2005.
- [25] L. Freitag, M. Grund, S. Singh, J. Partan, P. Koski, and K. Ball, "The whoi micro-modem: An acoustic communications and navigation system for multiple platforms," in *OCEANS, 2005. Proceedings of MTS/IEEE*, 2005.
- [26] S. Tang, D. Shinzaki, C. G. Lowe, and C. M. Clark, "Multi-robot control for circumnavigation of particle distributions," in *Proceedings of the International Symposium on Distributed Autonomous Robot Systems*, 2012.
- [27] B. V. Hight and C. G. Lowe, "Elevated body temperatures of adult female leopard sharks, *Triakis semifasciata*, while aggregating in shallow nearshore embayments: Evidence for behavioral thermoregulation?" *Journal of Experimental Marine Biology and Ecology*, vol. 352, pp. 114–128, 2007.